


# Characterization challenges for a cellulose nanocrystal reference material: dispersion and particle size distributions

Zygmunt J. Jakubek · Maohui Chen · Martin Couillard · Tianyang Leng · Leslie Liu · Shan Zou · Ulrich Baxa · Jeffrey D. Clogston · Wadood Y. Hamad · Linda J. Johnston 

Received: 22 December 2017 / Accepted: 15 March 2018 / Published online: 5 April 2018  
© Crown 2018

**Abstract** Cellulose nanocrystals (CNCs) have high aspect ratios, polydisperse size distributions, and a strong propensity for aggregation, all of which make them a challenging material for detailed size and morphology characterization. A CNC reference material produced by sulfuric acid hydrolysis of softwood pulp was characterized using a combination of dynamic light scattering (DLS), atomic force microscopy (AFM), transmission electron microscopy, and X-ray diffraction. As a starting point, a dispersion protocol using ultrasonication was developed to

provide CNC suspensions with reproducible size distributions as assessed by DLS. Tests of various methods for AFM sample preparation demonstrated that spin coating on a positively charged substrate maximizes the number of individual particles for size analysis, while minimizing the presence of agglomerates. The effects of sample-to-sample variability, analyst bias, and sonication on size distributions were assessed by AFM. The latter experiment indicated that dispersion of agglomerates by sonication did not significantly change the size distribution of individual CNCs in suspension. Comparison with TEM data demonstrated that the two microscopy methods provide similar results for CNC length (mean ~80 nm); however, the particle width as measured by TEM is approximately twice that of the CNC height (mean 3.5 nm) measured by AFM. The individual crystallite size measured by X-ray diffraction is intermediate between the two values, although closer to the AFM height, possibly indicating that laterally agglomerated CNCs contribute to the TEM width. Overall, this study provides detailed information that can be used to assess the factors that must be considered in measuring CNC size distributions, information that will be useful for benchmarking the performance of different industrially sourced materials.

**Electronic supplementary material** The online version of this article (<https://doi.org/10.1007/s11051-018-4194-6>) contains supplementary material, which is available to authorized users.

Z. J. Jakubek · M. Chen · T. Leng · L. Liu · S. Zou · L. J. Johnston (✉)  
Measurement Science and Standards, National Research Council  
Canada, Ottawa, ON K1A 0R6, Canada  
e-mail: Linda.Johnston@nrc-cnrc.gc.ca

M. Couillard  
Energy, Mining and Environment, National Research Council  
Canada, Ottawa, ON K1A 0R6, Canada

U. Baxa  
Electron Microscopy Laboratory, Frederick National Laboratory  
for Cancer Research, Frederick, MD 21702, USA

J. D. Clogston  
Nanotechnology Characterization Laboratory, Frederick National  
Laboratory for Cancer Research, Frederick, MD 21702, USA

W. Y. Hamad  
FPInnovations, 2665 East Mall, Vancouver, BC V6T 1Z4, Canada

**Keywords** Cellulose nanocrystals · Dispersion · Particle size distribution · Atomic force microscopy · Transmission electron microscopy · Dynamic light scattering · Biopolymer

## Introduction

Cellulose nanocrystals (CNCs) are one member of an emerging class of nanomaterials that are derived from cellulose, the most abundant biopolymer (Eichhorn 2011; Klemm et al. 2011; Moon et al. 2011; Dufresne 2013; Trache et al. 2017). Their generation from a renewable natural resource, increasing commercial-scale production, anticipated minimal toxicity and novel properties, and facile surface functionalization have led to many potential uses, some of which are now nearing commercial success (Kovacs et al. 2010; Shatkin et al. 2014, Shatkin and Kim 2015). The development of applications will require advances in characterization methods, standards, and reference materials to ensure comparability of materials from different biomass sources and producers, as well as continued studies to demonstrate that these materials can be used safely without negative effects on either human health or the environment (Davis et al. 2015). CNCs are spindle- or rod-shaped nanoparticles that have high aspect ratio and mechanical strength and low density and coefficient of thermal expansion; they form stable colloidal suspensions due to the negatively charged surface groups that are introduced during their extraction from cellulose biomass. Some of the key properties that must be characterized include size and shape, crystallinity, and surface functional groups. Measurement of CNC shape and size distribution is considerably more challenging than for well-behaved spherical nanoparticles with monomodal size distributions since they have an irregular rod-shaped structure, broad size distributions, and a strong tendency to aggregate or agglomerate. An important additional consideration is the requirement for dispersion of CNCs to provide suspensions with reproducible properties that are needed for various characterization methods.

Robust protocols for size and shape measurements using a range of particle counting and ensemble methods are available for spherical nanoparticles. Nanoparticle size is a method-defined parameter, and it is therefore important to consider the principle for each method and its specific advantages and limitations. Reference materials (typically with a mix of certified and reference values) are available for gold, silver, and silica nanoparticles, and they have been extensively used for method development and for

validation of measurement protocols and assessment of uncertainties through international inter-laboratory comparisons (Bonevich and Haller 2010; Meli et al. 2012; Rice et al. 2013; De Temmerman et al. 2014). However, there are still few studies where detailed examinations have been carried out for more complex “real-life” nanomaterials such as those produced industrially. Notable exceptions include recent studies where particle size distributions were assessed by TEM inter-laboratory comparisons for carbon black and titanium dioxide particles (Grulke et al. 2017). Note that these studies focused on detailed assessment of the size distribution and provided a full uncertainty analysis, an essential feature if one wishes to test for batch-to-batch similarity of materials or to compare different sources. Another recent study used a combination of particle counting, fractionation, and spectroscopy methods to evaluate the size distribution for a series of industrial nanomaterials with complex shapes and significant polydispersity and compared the results to those obtained for well-defined spherical and monodisperse quality control samples (Babick et al. 2016). This study was aimed at assessing the conditions under which the various materials could be classified as nanomaterials based on the European Commission recommendation.

Their particle shape, size polydispersity, and propensity for aggregation make CNCs a challenging material to analyze. The availability of a CNC reference material ([www.nrc.ca/crm](http://www.nrc.ca/crm)) provides one of the necessary components for method development and validation for this nanomaterial and for benchmarking the performance of different industrially sourced materials (Reid et al. 2017). Here, we report on the methods developed to characterize a CNC reference material, starting with protocols for preparation of suspensions with a reproducible size distribution as assessed by dynamic light scattering (DLS). Methods for depositing CNCs on solid supports for atomic force microscopy (AFM) were optimized to minimize particle agglomeration while maximizing the number of individual particles per image. The effects of sonication on the particle size distribution and the effects of analyst bias on image analysis were assessed by AFM. Finally, we compared particle size measurements from AFM and transmission electron microscopy, considering the merits and weaknesses of the two methods and discussing their relevance to ensemble measurements by DLS and X-ray diffraction.

## Materials and methods

### Materials

CNC was a National Research Council Canada-certified reference material (CNCD-1, ([www.nrc.ca/crm](http://www.nrc.ca/crm))). The CNC was produced by CelluForce, Inc., Windsor, QC, by sulfuric acid hydrolysis of softwood pulp followed by neutralization and sodium exchange, purification, and spray drying. The material was homogenized, subsampled in 2 and 10 g units into pre-cleaned screw-capped glass bottles, and sterilized by gamma irradiation to a minimal dose of 10 kGy at the Canadian Irradiation Centre (Laval, QC). The homogeneity of the material was evaluated by DLS of suspensions prepared using the standard protocol described below. The short-term stability of dry CNC and 2% mass fraction suspensions was also evaluated by DLS. Long-term stability was assessed by DLS and conductometric titration for material stored at  $5 \pm 2$  °C for 2 years.

### CNC dispersion and sonication

Previous studies have shown that the sonication efficiency for CNC is optimal for 2% mass fraction CNC suspensions (Beck et al. 2012). The protocol used to prepare 2% mass fraction sonicated CNC suspensions is summarized in the Supporting Material. The CNC size was assessed by DLS as a function of applied sonication energy. These experiments used a 130 W ultrasonic processor (EW-04714-50, Cole-Parmer) equipped with a ¼ inch tip probe (EW-04712-14 Cole-Parmer). The amplitude was set at 50% and the processing was done with continuous sonication, which resulted in the average power provided to the probe in the (10 to 11) W range. The total energy transfer efficiency for the sonicator used is 0.97, as measured calorimetrically (Taurozzi et al. 2011). Pulsed operation of the ultrasonic processor indicated, primarily at low applied energies, dependence of the average size on the fraction of *time on* and resulted in a wider sample-to-sample variation in the average size. The average CNC size and size distribution varied with the processed sample concentration even when the sonication energy divided by mass of CNC was kept constant. This confirms the importance of selecting a fixed concentration for preparation of CNC suspensions for size measurements (Beck et al. 2012). Therefore, 2% mass fraction CNC suspensions were used for all experiments.

### Dynamic light scattering

Samples for DLS measurements were prepared by diluting the 2% mass fraction CNC suspensions to 0.1% using deionized water and then adding 1 mL of 10 mM NaCl solution to 1 mL of 0.1% mass fraction CNC suspension to obtain 2 mL of 0.05% mass fraction suspension in 5 mM NaCl. The 0.05% suspension was used within several hours of preparation and was shaken vigorously before transfer to the DLS cell. The suspension was drawn into a microsyringe and filtered through a 13-mm-diameter 0.45- $\mu$ m PVDF membrane syringe filter (Millex-HV, MilliporeSigma), and the first 3 drops were discarded before placing a minimum of 50  $\mu$ L in the bent capillary DLS cuvette (DTS1061, Malvern).

The 0.05% suspensions were analyzed with a Zetasizer Nano ZS (red) (Malvern) using a 632.8-nm HeNe laser and signal detection at 173°. The 0.05% suspensions were usually analyzed immediately after preparation except when multiple samples were prepared simultaneously, in which case the last samples in the batch were analyzed up to 4 h following their preparation. The measurements of Z-average and polydispersity index (PDI) were done at 25 °C with values for viscosity and refractive index of dispersant of  $\eta = 0.8872$  cP and  $n = 1.330$ , respectively, and automatic positioning and attenuation selection set on. Each sample was equilibrated for 180 s, and three measurements, each consisting of ten runs of 10 s, were acquired. Each measurement was analyzed using Zetasizer software (ver. 7.11) by the method of cumulants with the general purpose model. The data were processed to obtain a three-measurement average value and a standard deviation for Z-average and PDI of each sample. Prior to the measurements, the instrument operation was positively qualified by measuring the ERM-FD304 (JRC-IRMM) reference material to obtain Z-average and the corresponding 95% expanded uncertainty equal to  $41.4 \pm 0.6$  nm, compared to the certified value of  $42.1 \pm 0.6$  nm.

### Atomic force microscopy

CNC 2% mass fraction sonicated suspensions were diluted 500-fold, vortex-mixed for 5 s, and spin-coated on a mica substrate. A freshly cleaved mica substrate (1 in.  $\times$  1 in.) was coated with 0.01% mass fraction poly-L-lysine (PLL) solution (Sigma-Aldrich) to provide a

positively charged surface. A 200- $\mu\text{L}$  aliquot of PLL solution was added onto the mica substrate, which was then covered with a petri dish for 10 min. The mica substrate was rinsed with deionized water five times and dried in a nitrogen stream. For spin coating, 200  $\mu\text{L}$  of the freshly diluted CNC suspension was hand shaken for a few seconds and pipetted onto the center of a freshly prepared PLL-mica substrate, which was vacuum mounted onto a spin coater (WS-650SZ-6NPP/LITE, Laurel). The CNC suspension covered most of the substrate except for small areas at the four corners. The spin coating was performed immediately using static mode at 4000 rpm for 25 s, with an acceleration rate of 2000 rpm/s. Five independent CNC samples were deposited, each from a separate suspension prepared by the standard dispersion protocol.

The CNC-PLL-mica sample was mounted to a microscope slide for imaging with an atomic force microscope (NanoWizard II, JPK Instruments). Intermittent contact mode was used with a silicon AFM tip (HQ:XSC11/AL BS, MikroMasch; typical radius 8 nm, 2.7 N/m spring constant). Large-sized images (5  $\mu\text{m} \times 5 \mu\text{m}$  or 10  $\mu\text{m} \times 10 \mu\text{m}$ ) were recorded to verify the overall morphology and homogeneity of the CNC samples. A series of 1  $\mu\text{m} \times 1 \mu\text{m}$  AFM images was then acquired with a size of 512 pixels  $\times$  512 pixels, a scan rate of 0.8 to 1.0 Hz, and a Z-piezo range of 1.5  $\mu\text{m}$ . The images were collected from different areas close to the center of the substrate without prior imaging of the larger areas used to locate regions with suitable CNC density. To minimize compression of particles by the tip, the ratio between the amplitude setpoint ( $A_{\text{sp}}$ ) and the free amplitude ( $A_0$ ) was set to  $\sim 0.8$ – $0.9$ . In our experiments, when the ratio was adjusted to  $> 0.92$ , the AFM probe started losing track of the CNC features, causing unstable imaging. Selected samples were imaged using different setpoint values to estimate the uncertainty contribution due to amplitude variation resulting in a variation of applied force (see Fig. S1).

Prior to imaging CNC samples, the AFM was calibrated using four-step height standards (VLSI Standards, Inc.; STS3 series; 18, 44, 100, and 180 nm). Instrument operation was qualified, and the method was validated by measuring nanoparticle reference materials ERM-FD102 (JRC-IRMM), RM 8011 (NIST), and RM 8013 (NIST), for which the measured nanoparticle diameter values were all within the combined expanded uncertainty of the certified values.

Images were flattened using a first-order polynomial fit using the JPK AFM software before processing using Gwyddion 2.35 (Czech Metrology Institute) for height and length analysis. For each image, all single particles were selected and their length and height measured. Particles adjacent to each other were only selected for analysis if the separation between the particles was clearly established in the contact or near-contact areas. Particles crossing or touching an edge of the image, particles  $< 25$  nm long, particles crossing each other, and particles with imaging artifacts were excluded. The “extract profiles” function (thickness setting of 3 pixels) was used to measure the profiles for all individual CNCs. A profile was drawn along the long axis of the particle, and an average background level was determined (Fig. S2). The slopes defined by the first four or five points that deviate from the background level on either side of the CNC profile were extrapolated to intersect the background level. The distance between the two intersection points was measured to give the CNC length. No correction for tip convolution was applied. The height was measured as the difference between the vertical displacement at the highest region of the profile, ignoring any single point spikes, and the adjacent background.

The similarity of height and length data sets obtained from different samples, analysts (two), and sonication conditions was assessed using the following nonparametric statistical methods that are appropriate for data sets that are drawn from not-normally distributed populations or for which the normality of a population cannot be verified: Kruskal-Wallis ANOVA to compare the distribution widths, Mood’s median to compare the medians of the two distributions, and two-sample Kolmogorov-Smirnov tests to compare the widths and medians of the distributions.

#### Transmission electron microscopy

CNC size and size distribution were studied by TEM in two laboratories with five independently prepared samples analyzed by lab 1 and three samples by lab 2. For lab 1, samples were prepared by diluting 2% CNC suspensions 100-fold with deionized water and depositing on plasma-exposed (2 min, Fischione model 1070) carbon film-covered copper grids (200 mesh, 01840-F, Ted Pella). One drop of CNC suspension was deposited on the grid for 4 min and wicked with a filter paper. The sample was washed by adding one drop of deionized

water to the grid and wicking with a filter paper after a few seconds. Finally, the sample was stained by depositing a drop of 2% uranyl acetate solution on the grid for 4 min and wicking away the solution with a wet filter paper. The grid was left to air-dry before insertion into the microscope. Images were recorded with a Titan<sup>3</sup> 80-300 (FEI) transmission electron microscope operated at 300 kV and  $\times 27,000$  magnification. The microscope calibration was verified by imaging a TEM magnification calibration standard (MAG\*I\*CAL, EMS).

For lab 2 imaging, CNC suspensions were deposited onto freshly glow-discharged carbon-coated grids for 30 s, rinsed with water, and negatively stained with 0.7% uranyl formate. Images were recorded with a  $2000 \times 2000$  CCD camera (Advanced Microscopy Techniques) on an H7600 (Hitachi) microscope operated at 80 kV and  $\times 15,000$  and  $\times 30,000$  magnifications. Prior to CNC imaging, 10-nm gold nanoparticles (RM 8011, NIST) were deposited on carbon-coated grids, dried, washed five times, and imaged with the microscope operated at 80 kV and  $\times 40,000$  and  $\times 80,000$  magnifications. Analysis of 200 gold nanoparticles gave an equivalent mean diameter of 8.6 nm (0.05 nm standard deviation of the mean) compared to the reference value of  $8.9 \pm 0.1$  nm.

TEM images were analyzed using a custom ImageJ (National Institutes of Health) macro. For each image, single particles were selected and their length and width measured. Particles crossing one another were selected for analysis only if they crossed at an angle in the approximate range of  $30^\circ$  to  $90^\circ$ , and there was a clear indication that the crossing particles can otherwise be considered as single ones. Those crossing at an angle outside the range specified above or adjacent to each other were selected for analysis only if the separation between the particles was clearly established in the contact areas. The length was measured in a straight line between the furthest points independent of asymmetry or slight curvature of the particles. The width of the particles was typically measured at the midpoint of their length unless a particle was clearly asymmetric; the width of asymmetric particles was measured at the widest point.

### X-ray diffraction

Crystallinity was measured by X-ray diffraction using a D8 Advance X-ray diffractometer (Bruker), in Bragg-Brentano configuration, with copper  $K\alpha_1$  and  $K\alpha_2$

radiation, a nickel filter (to remove  $\text{CuK}\beta$ ), a LynxEye silicon strip detector, and 1-mm divergent, 8-mm anti-scatter,  $2.5^\circ$  Soller slits. The generator was operated at 40 kV and 40 mA. Thin film samples of CNC on silicon were prepared by drop casting of a 2% CNC suspension. The spectra were fit to a cellulose I structure with deconvolution using Ruland-Rietveld analysis (Hamad and Hu 2010). The crystalline fraction was obtained as the ratio of the total deconvoluted crystalline regions relative to the sum of crystalline and amorphous regions in the X-ray diffraction spectrum. The crystallite size was determined using the Scherrer equation with the constant  $K$  set to 1

$$D = \frac{K\lambda}{\beta \cos\theta} \quad (1)$$

where  $D$  is the “apparent crystallite size” and  $\beta$  the full width of the diffraction peak measured at half maximum (FWHM) height of the instrument-corrected line profile.

## Results

### Dispersion of CNCs

Dry CNCs are heavily agglomerated, typically having large micron-sized particles that are difficult to redisperse. In fact, surface area measurements of dry CNCs using the Brunauer-Emmett-Teller (BET) method give very small values ( $\sim 1.3 \text{ m}^2/\text{g}$ ), more than 2 orders of magnitude lower than values estimated from the dimensions of individual particles (Brinkmann et al. 2016). A reproducible procedure that disperses the material in water to give stable suspensions with minimal aggregation or agglomeration is an essential first step for developing reproducible characterization methods and applications. Typical procedures for dispersion of nanomaterials rely on the use of dispersants or ultrasonication to eliminate or minimize agglomerates (Taurozzi et al. 2011). Here and in our earlier study (Brinkmann et al. 2016), we have adapted a procedure reported by Beck and coworkers, who examined the effect of the counterion, water content, drying method, and concentration on the redispersion of CNCs (Beck et al. 2012). CNC suspensions were prepared as described in the “Materials and methods,” and dynamic light scattering was used to assess the particle size as a function of sonication energy. Note that the Z-average

measured by DLS provides the diameter of an equivalent sphere that has the same diffusion coefficient as the rod-shaped CNC particles. Although the Z-average cannot be used to measure either length or cross section directly unless the other dimension is known, it does provide a useful method for rapid evaluation of changes in particle size for relatively large numbers of samples for which microscopy measurements would be prohibitively time-consuming.

Figures 1 and S3 illustrate the variation in Z-average and polydispersity for CNC suspensions as a function of applied sonication energy on a log and linear scale, respectively. These figures summarize data from nine experiments carried out by four people at different times over a period of approximately 18 months. Five experiments probed the effects of sonication energy on independently prepared CNC suspensions. Data for four experiments at a single sonication energy that were used to demonstrate sample homogeneity and stability are also included. The CNC Z-average decreases rapidly with increasing sonication energy, up to approximately 2 kJ/g (Fig. S3). At higher energies, the size changes relatively slowly. However, even at energies as high as 20 kJ/g, Z-average continues to decrease with increasing sonication energy, as evident from the log-linear plot (Fig. 1b). The log-linear plot of Z-average in Fig. 1 clearly indicates (see guidelines) that the mean size variation of CNCs as a function of sonication energy above 0.5 kJ/g is approximately governed by a power law with a change of exponent value at approximately 4 kJ/g. The change in slope at higher energies may reflect slower disruption of more tightly packed aggregates. Previous studies have concluded that CNC damage does not occur over this range of sonication energies (Beck et al. 2011; Shafiei-Sabet et al. 2012). The sample polydispersity shows a similar dependence on sonication energy. However, due to the larger relative errors for PdI, the trends are less clear than those for Z-average. Note that the points at sonication energies below 0.5 kJ/g deviate from the bi-exponential dependence, which reflects sample-to-sample variation of the extent of initial CNC agglomeration due to differences in water content of the dry CNCs or the sample dispersion procedure, as well as the larger relative uncertainty of the applied sonication energy.

The effect of sample filtering was also examined as a function of applied sonication energy. As shown in Fig. S4, the measured Z-average values were similar for samples that were unfiltered and filtered (0.45- $\mu$ m

filter) prior to DLS analysis. The differences were within the uncertainty for the measurement (see below). The variation in PdI for the two sample preparation methods was larger.

Based on the dependence of Z-average on sonication energy illustrated in Fig. 1, a value of 4850 J/g was selected for preparation of standard CNC suspensions for measurements of particle size distribution. The selected sonication energy is a compromise between minimizing the total energy applied to the samples, while selecting a value beyond which the size change with added sonication energy is small. During the characterization of the reference material, a total of 86 independently prepared suspensions (from 18 different units of CNC-D-1) were analyzed by DLS as part of the demonstration of material homogeneity and stability and during microscopy characterization and determination of the sulfate half ester content. The combined data are shown in Fig. 2. The data were analyzed for various trends and within-bottle and between-bottle homogeneity using an unbalanced ANOVA method. Contributions due to DLS repeatability and intermediate precision, between-bottle inhomogeneity, short-term suspension stability, variation in sonication energy, and calibration were included in the evaluation of standard uncertainty. A trueness contribution was evaluated for Z-average from measurements of a certified reference material, and the long-term (dry CNCs) stability contribution was assessed to be negligible compared to other components. The final values for the mean and its expanded uncertainty ( $k = 2$ ) were  $70.0 \pm 1.4$  nm for Z-average and  $0.180 \pm 0.003$  for polydispersity. The total data set demonstrates the repeatability and intermediate precision of the dispersion procedure, as assessed using Z-average as a measure of the particle size distribution.

#### Height and length analysis by AFM

AFM studies of CNCs have typically imaged samples deposited on mica that is coated with poly-L-lysine to immobilize the negatively charged particles (ISO 19716: 2016). The most frequent approach of incubating the support with a dilute aqueous CNC suspension and washing to remove loosely adhered particles typically results in agglomeration of the individual particles, independent of whether there are agglomerated particles in the initial suspension. Although agglomeration can be reduced by careful optimization of the CNC concentration and the incubation and wash procedures, it cannot

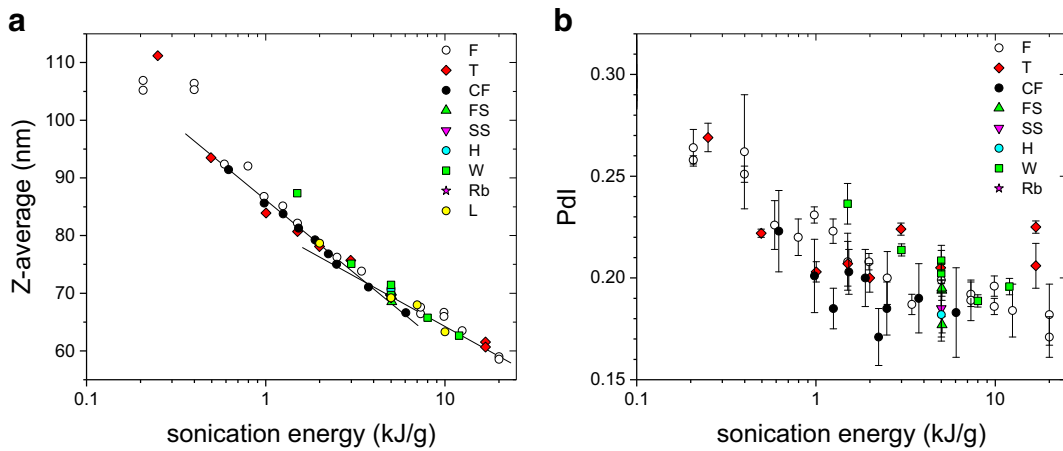


**Fig. 1** Z-average (a) and polydispersity index (Pdl, b) as a function of sonication energy divided by mass of CNCs (kJ/g) plotted on log-linear scales. Symbols corresponding to different series of measurements vary by color and shape. Error bars correspond to 1

standard deviation of three DLS measurements for each sample. The error bars for most of the Z-average points are obstructed by the symbols. The thin solid lines in the Z-average plot (a) are shown to indicate approximately linear trends for data points

be eliminated. Here, we have examined an alternate spin coating method that has been reported to be advantageous for preparation of other nanoparticle samples (Hoo et al. 2010; Delvallee et al. 2016). After optimization of the volume and concentration of CNC suspension and the spin rate and time, it was possible to achieve a more uniform CNC distribution and a larger fraction of individual, non-agglomerated particles than could be obtained by the incubation method.

Representative AFM images are shown in Fig. 3 for samples prepared by the incubation and spin coating methods. Although there is a higher particle density for the sample prepared by spin coating, it is still

possible to obtain a larger number of individual CNCs for size analysis than for samples prepared by incubation. For comparison, an average of 17 particles/image was obtained by the incubation procedure whereas with spin coating, an average of 24 particles/image was typical. Multiple images were collected and analyzed for five samples deposited by spin coating on PLL-coated mica. A sufficient number of images (typically 12–14 images per sample) to yield at least 300 individual particles/sample were collected. All individual particles were analyzed manually using Gwyddion (see “Materials and methods”), excluding clustered particles, particles that touched the edge of the image, and particles

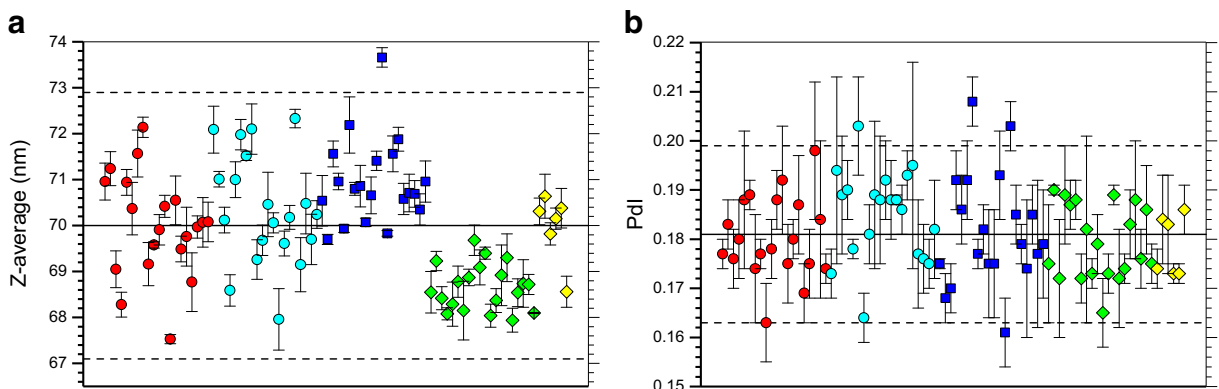


**Fig. 2** Z-average (a) and polydispersity index (Pdl, b) measured by DLS for CNC suspensions sonicated with an energy of 4850 J/g. Symbols corresponding to different series of measurements vary by color and shape. Error bars correspond to 1 standard deviation

of three DLS measurements for each sample. Solid black lines indicate the average values of 86 measurements. Broken black lines indicate the average value plus/minus  $k = 2$  expanded uncertainty of a single data point

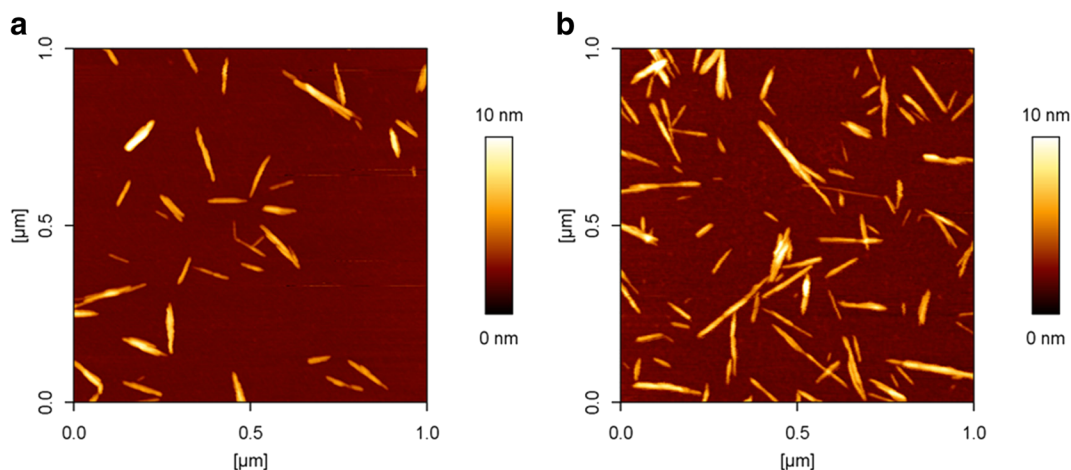


**Fig. 3** AFM images of CNCs deposited on poly-L-lysine-coated mica by incubation (a) and spin coating (b) methods

that were <25 nm in length or had obvious imaging artifacts.

The selection of analyzable particles (individual CNCs) is somewhat subjective, and different analysts may select and analyze a slightly different subset of particles, resulting in differences in the average height and/or length of the particles as noted in our previous work (Brinkmann et al. 2016). To address the possibility of analyst bias with a larger data set than previously examined, the images from each of the five samples were analyzed independently by two analysts. Height and length histograms for each of the five samples are shown in Figs. S5 and S6 for analysts 1 and 2, respectively. The means and distribution widths for each sample/analyst are summarized in Table S1 and Fig. S7.

Individual data sets for each sample and each analyst, for both length and height, were pairwise tested by the Kolmogorov-Smirnov and Kruskal-Wallis ANOVA and Mood's median tests. The tests indicated that for approximately half the data set pairs (both between samples and between analysts), the populations from which the data sets were drawn were significantly different at the 0.05 level; for a few pairs, the tests were inconclusive. Comparison of the analyzed images demonstrated that the two analysts generally counted the same particles. However, there were typically a small number of particles that were counted by only one analyst; often, these were larger particles where there was more uncertainty as to whether or not the "particle" corresponded to a single CNC or two agglomerated CNCs. It appears that this makes a significant contribution to the analyst-analyst variation. Overall, the data showed that there are significant experimental (sample heterogeneity, sample

preparation, image recording, acquisition, etc.) and analyst effects, which contribute to the overall uncertainties for mean length and height. However, a review of the sample preparation, image acquisition, and data analysis provided no reason for rejection of any particular data set. The final mean values for height and length were calculated in a two-step process. First, for each sample/analyst data set, the mean value and standard deviation were calculated. Next, the five data set means for each analyst were used to calculate the analyst mean of means (Table 1). The combined histograms for the five samples for each analyst are shown in Figs. 4, S5, and S6. Although the combined length data have similar means for the two analysts, there is a larger difference between the mean heights for the two analysts (3.4 and 3.7 nm), which probably reflects analyst bias in the selection of individual particles, as discussed above.

**Table 1** Summary of CNC particle size distributions from AFM and TEM analysis

| Experiment     | Height (AFM) or width (TEM) (nm) |           | Length (nm) |          |
|----------------|----------------------------------|-----------|-------------|----------|
|                | Mean                             | <i>W</i>  | Mean        | <i>W</i> |
| AFM, analyst 1 | 3.4 ± 0.8                        | 1.1 ± 0.4 | 76          | 32       |
| AFM, analyst 2 | 3.7 ± 0.6                        | 1.2 ± 0.4 | 78          | 30       |
| AFM, combined  | 3.5 ± 0.7                        | 1.1 ± 0.5 | 77          | 31       |
| TEM, lab 1     | 7.5                              | 2.0       | 82          | 36       |
| TEM, lab 2     | 7.2                              | 1.6       | 92          | 33       |

Mean and *W* are the average value and the width of the corresponding distribution of height, width, or length. Uncertainties, where shown, are 95% expanded uncertainties



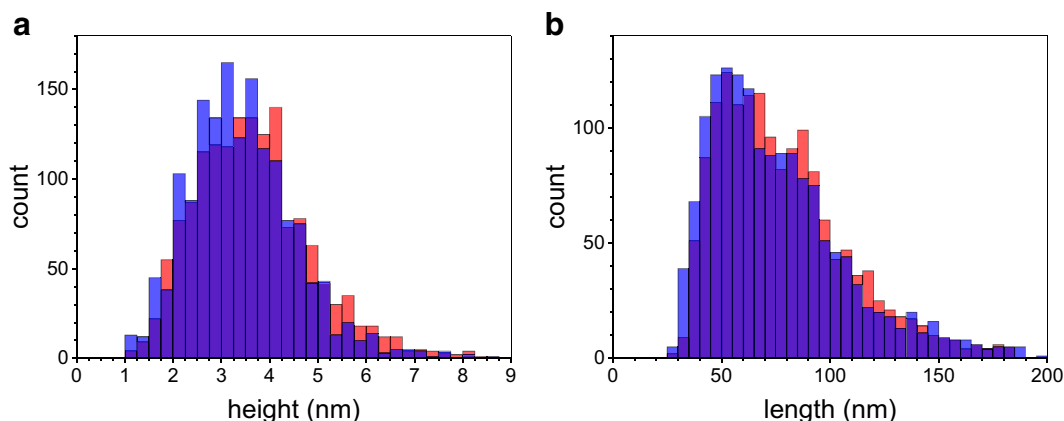


**Fig. 4** Histograms for AFM height (**a**) and length (**b**) as measured by analyst 1 (blue) and analyst 2 (red). Overlapping parts of histograms are shown in violet

For comparison, the analyst means were averaged to obtain the grand means for height and length (Table 1); the histograms for the combined data for the two analysts are shown in Fig. S8.

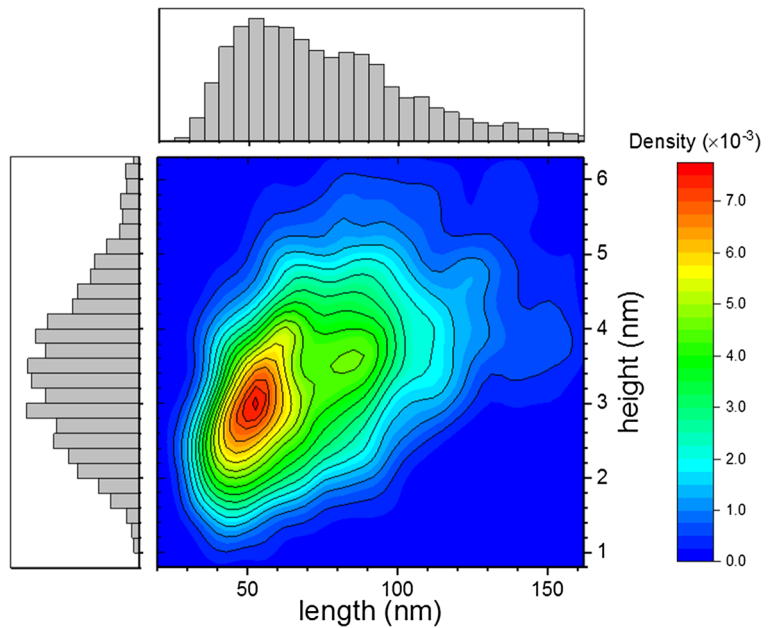
The individual length and height data sets for the five samples and two analysts were tested for fits to lognormal and Weibull distributions which are typically used to fit data for particles synthesized in the liquid phase and for particles produced by a milling or crushing process, respectively. Both distributions were rejected for most of the data sets by modified Kolmogorov-Smirnov and Anderson-Darling goodness-of-fit tests using OriginPro 2017. In a few cases, the tests were inconclusive. The lack of fit for the length distribution is expected as evidence for a multimodal distribution is apparent in the histograms (see Fig. 4).

Recent reports have illustrated the utility of two-dimensional (2-D) plots of descriptors (e.g., size-size or size-shape) for obtaining additional morphological information for asymmetric particles (Grulke et al. 2017). As an alternate approach for visualizing the CNC data, we examined the 2D kernel density plot of height vs. length for the combined data sets from both analysts (Fig. 5). The 2D plot provides a clear indication for the presence of multiple populations. The global maximum is observed at a CNC height of  $\sim 3$  nm and a length of  $\sim 52$  nm, and there is a positive correlation between length and height. The kernel density plot also indicates that CNC particles longer than  $\sim 100$  nm have heights of  $\sim 4$  nm and show less variation with particle length. The evidence for small populations of larger particles could be explained either by the inherent variability in the hydrolysis process that liberates individual

CNCs from the larger fibrils or by particle aggregation. Although the presence of hydrogen-bonded side-by-side particles may be difficult to distinguish from single CNCs and may lead to heterogeneity in measured widths/heights, it seems unlikely that there are a significant number of end-to-end CNC dimers or oligomers that could contribute to length heterogeneity. This suggests that the population heterogeneity is more likely to reflect the initial hydrolysis process.

The effect of sonication on the average particle size was also assessed by AFM for comparison with DLS data and to investigate whether dispersing CNC aggregates changed the measured particle size distribution for individual CNCs. CNC suspensions were sonicated at 0, 2, 5, 7, and 10 kJ/g and then diluted and deposited on PLL-coated mica and imaged by AFM. The number of aggregates/image was larger for the unsonicated sample, consistent with the larger Z-average observed for unsonicated samples or those sonicated with low energies ( $< 0.5$  kJ/g). The variation in the mean values for height and length for these samples was similar to the variation observed between individual samples or between analysts (Fig. 6; compare Table S2 to Table S1). ANOVA showed that at the 0.05 level, the five data sets were drawn from significantly different populations. Upon exclusion of the data set for the sample sonicated with 7 kJ/g energy, further analysis showed that the remaining data sets were drawn from the same population. Also, no trends as a function of sonication energy were found and the observed scatter between mean values and medians for the five samples was similar to those observed for the length and height of the samples sonicated with 4.85 kJ/g energy. The AFM protocol

**Fig. 5** Two-dimensional kernel density plot of CNC height vs. length for the combined set of AFM measurements for over 1500 particles from five samples and independently analyzed by two analysts. Height (left, bin size 0.2 nm) and length (top, bin size 5 nm) histograms are also shown



specifies measurement of individual particles only, excluding aggregates from the analysis. The lack of change in either the length or height of the individual particles as a function of sonication energy is in contrast to the DLS results where sonication leads to a decrease in Z-average. We conclude that the size distribution of particles within the CNC aggregates or agglomerates that can be dispersed by sonication is indistinguishable from the size distribution of individual particles present in the initial suspension, within the limits of our current methods. The results further support an earlier conclusion that sonication does not lead to significant breakage of individual particles, based on the observation that the same dimensions were measured by TEM for samples sonicated with 1 and 3 kJ/g (Shafiei-Sabet et al. 2012). By contrast, we have previously reported a modest increase in length for a single sample of never-dried CNC after sonication (Brinkmann et al. 2016). The present results, which are based on a more extensive data set, indicate that this is unlikely to be the general case, although one cannot rule out the possibility that different samples do not show the same behavior.

Finally, we estimated the combined uncertainty associated with height measurements for CNCs. A similar analysis was not attempted for length, since the data have not been corrected for tip convolution effects. A deconvolution procedure is not straightforward to implement since multiple tips are typically required for a single sample and since the tip shape and size is likely to

change during imaging. The combined uncertainties of the height and the width of the height distribution were estimated as follows. First, for each sample and analyst height data set, uncertainties of the mean and corresponding standard deviation of the distributions were calculated. Data set-specific combined uncertainties included (1) uncertainty of the calibrated mean height with contributions from the standard error of the mean and the vertical coordinate calibration, (2) uncertainty in the selection of the background and maximum particle height levels due to noise and substrate and particle roughness, and (3) uncertainty due to set point adjustment (estimated at 0.19 nm and the largest contribution to the data set-specific mean height value combined uncertainties). Next, between samples, mean values of height and width of height distribution were calculated for each analyst. Corresponding sample-specific uncertainty included data set-specific uncertainties, and a sample bias contribution expressed as a standard deviation of the five sample means. The final uncertainty for analyst 1 is larger than that for analyst 2 (Table 1), reflecting the larger sample-to-sample standard deviation.

Since we established that both analysts measured largely the same particles, the uncertainty related to analyst bias could be estimated using the following simple approach. For each sample, we calculated a difference between sample mean height values and distribution width values obtained by both analysts ( $\Delta_i$ ,  $i =$

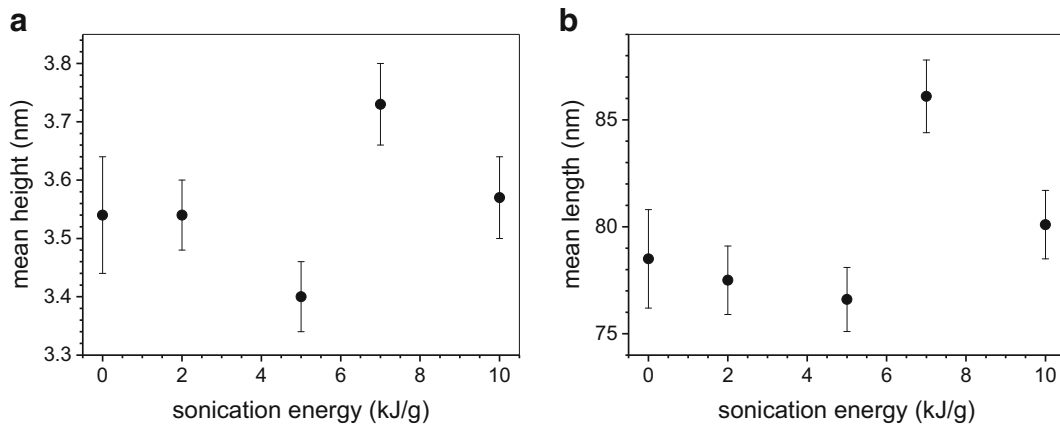


**Fig. 6** Mean values of height (a) and length (b) of CNC particles measured by AFM as a function of sonication energy. Error bars are 1 standard error of the mean

1, ..., 5). We also assumed that analyst-specific errors are normally distributed with variances equal to  $\delta_1^2$  and  $\delta_2^2$  for analyst 1 and analyst 2, respectively. Consequently, the variance of the between analyst differences ( $\Delta_i$ ) is equal to the sum of analysts' bias variances,  $\delta^2 = \delta_1^2 + \delta_2^2$ . Approximating  $\delta$  with a standard deviation ( $s_a$ ) of the five sample between analyst differences ( $\Delta_i$ ), we expressed the average uncertainty due to a single analyst bias as  $s_a/\sqrt{2}$ . This combined analysis for five samples and two analysts gives final values of  $3.5 \pm 0.7$  and  $1.1 \pm 0.5$  nm for the mean height and the corresponding distribution width (Table 1). Comparison to the values reported in the certificate for CNCD-1 (analyst 1, Table 1) shows good agreement and indicates that inclusion of data from multiple analysts has a small effect on the mean height and distribution width.

### Transmission electron microscopy

CNCs were deposited on carbon-coated copper grids and stained with uranyl acetate. The air-dried samples were imaged by TEM with a collection of a large number of images for analysis of the length and width of individual particles (i.e., excluding agglomerates and touching particles unless the outlines of the individual particles could be readily determined). Five suspensions (the same as those used for AFM analysis) were imaged in lab 1 and an additional three samples were imaged in lab 2. Figure 7 shows representative images, which illustrate the significant level of aggregation that was typical for these samples. The high-resolution image shown in Fig. 7 illustrates two adjacent particles which

could be mistakenly assigned as a single particle at lower resolution.

Histograms for the combined length and width data from all samples for lab 1 are shown in Fig. 8; the mean and distribution width (standard deviation) for both length and width for each sample are summarized in Table S3. The average length and width obtained from the combined data set are shown in Table 1. The average length is slightly longer ( $\sim 5$  nm) than that measured by AFM, despite the fact that the AFM value is anticipated to be an overestimate due to tip convolution effects. The average TEM width of 7.5 nm is approximately twice the value measured for the AFM height (3.4 nm), consistent with our earlier TEM study of a different CNC sample. The standard deviation of the TEM-measured width distribution (2.0 nm) is considerably larger than the standard deviation of the AFM-measured height distribution (1.0 nm). This might be interpreted as consistent with significant lateral aggregation of CNC particles in the TEM images. However, the relative standard deviation (standard deviation divided by the mean width) of the TEM-measured width distribution ( $\sim 0.27$ ) is actually somewhat smaller than the relative standard deviation of the AFM-measured height distribution ( $\sim 0.32$ ), which argues against a significant number of side-by-side aggregates for these samples. It is important to consider whether compression of individual CNCs by the AFM tip could account for the small AFM height, relative to the TEM width. Although it is clear that the particles are compressed as the imaging force increases, tests using variable setpoints indicate that height decreases are within the 0.5–1 nm range and cannot account for the observed factor of two discrepancies

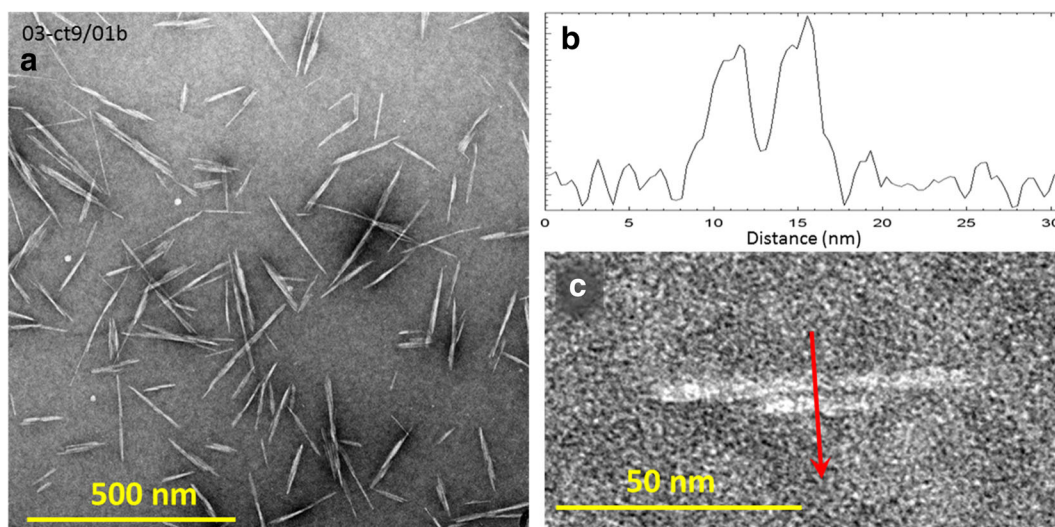


**Fig. 7** TEM images of CNCs (**a**, **c**). The high-resolution image (**c**) and cross section (**b**, measured along the red line in **c**) show two individual particles

between AFM height and TEM width. Uncertainty in the measured TEM width may be introduced by the poor contrast and difficulties in defining the edge of the particle. However, this is likely to increase the TEM width, rather than reduce it. Experiments in which CNC width is measured by AFM, either with implementation of a deconvolution approach (Postek et al. 2011) or using very sharp tips, may be required to resolve this issue.

Figure 8 shows the 2D kernel density plot of width vs. length for the TEM data. The plot is similar to that for AFM as there is a clear positive correlation between length and width with a maximum at a width of  $\sim 7.2$  nm and a length of  $\sim 55$  nm. However there are no density maxima associated with multiple populations, possibly because the individual histograms for both length and width are significantly noisier than those for AFM, even though the total number of particles analyzed is larger by  $\sim 25\%$ . Histograms of AFM and TEM measurements are compared in Fig. S9, clearly illustrating the difference in cross section measured by the two methods. The length histograms for the two methods are similar, consistent with the small differences between the measured distribution widths.

TEM data for three samples were measured independently at a second lab in order to test whether a similar large variation would be obtained between the measured AFM height and TEM width. The data are summarized in Table S3, with width and length histograms shown in Fig. S10. The combined data (Table 1) indicate that the

mean length for the lab 2 data set is larger than that from lab 1, while the width is slightly smaller. The shapes of the histograms vary considerably between the two labs, particularly for length. Interestingly, the 2D kernel density plot (Fig. S10) does not indicate a positive correlation between length and width. Although the lab 2 data set indicates that the  $\sim 7.5$  nm mean width can be reproduced, the lack of correlation between length and width is puzzling. Possible explanations for these results include differences in sample preparation or image resolution between the two labs and effects of the limited size of the data set for lab 2 (600 particles).

### X-ray diffraction

For comparison to particle counting and ensemble DLS measurements, we have also used X-ray diffraction to provide information on the primary crystallite size. Figure 9 shows a representative spectrum for a thin film sample of evaporation-induced self-assembled (EISA) CNCs. The spectra for five thin film EISA samples, each prepared from a separate CNC suspension, were recorded. The spectra were fit to a cellulose 1 structure with deconvolution using Ruland-Rietveld analysis (Hamad and Hu 2010). The crystalline fraction is obtained as the ratio of the total deconvoluted crystalline regions divided by the sum of crystalline and amorphous regions in the X-ray diffraction spectrum and was estimated as 0.88 (standard deviation of 0.02). The crystallite size was estimated, using the Scherrer equation (Eq. 1), to be

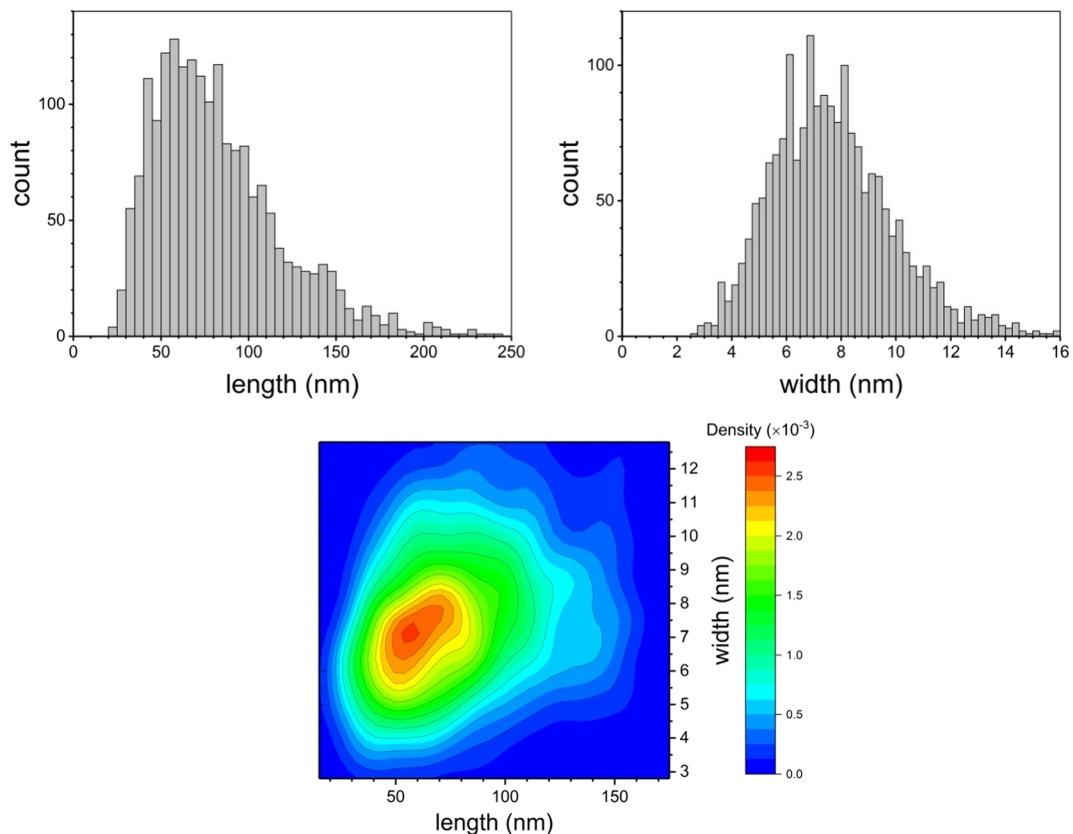


**Fig. 8** Combined histograms of CNC length and width (both in nm) as measured by TEM for five samples (lab 1) and 2D kernel density plot for CNC width vs. length

4.8 nm (standard deviation = 0.02), which is similar to literature values for CNCs derived from wood pulps (Hamad and Hu 2010; Jiang et al. 2010).

## Conclusions

This study has examined some of the considerations for evaluation of CNC particle size distributions using several methods. As an important first step, we demonstrate that it is possible to reproducibly disperse dry CNCs to obtain samples with the same apparent size distribution, measured as an equivalent hydrodynamic diameter by DLS. It is important to keep in mind that the measured Z-average does not provide either the length or width of the particles but is rather an apparent “size” and that it measures all particles (individual CNCs and their aggregates and agglomerates) with stronger weighting of large particles since the scattering intensity is proportional to the sixth power of particle size. Nevertheless, the ability to obtain samples with a reproducible Z-

average (over a period of time and by multiple people) gives confidence that the method produces similar CNC samples without the requirement for time-consuming microscopy experiments. Several recent investigations have used field flow fractionation and a multistage separation with layered filter membranes to fractionate polydisperse CNC samples; these studies started with samples with a much broader range of particle lengths than those measured for the sample studied here (Guan et al. 2012; Hu and Abidi 2016). Nevertheless, it would be of considerable interest to attempt to fractionate the sample used in our study, particularly to assess the extent of aggregates in the sample after sonication using our standard protocol.

Detailed studies of the CNC particle size distribution by AFM have been used to assess sample-to-sample variability, effects of analyst on the image processing, and effects of sonication. Overall, the results demonstrate that uncertainty components due to both analyst subjectivity in image analysis and sample-to-sample variability (due to either unit-to-unit differences

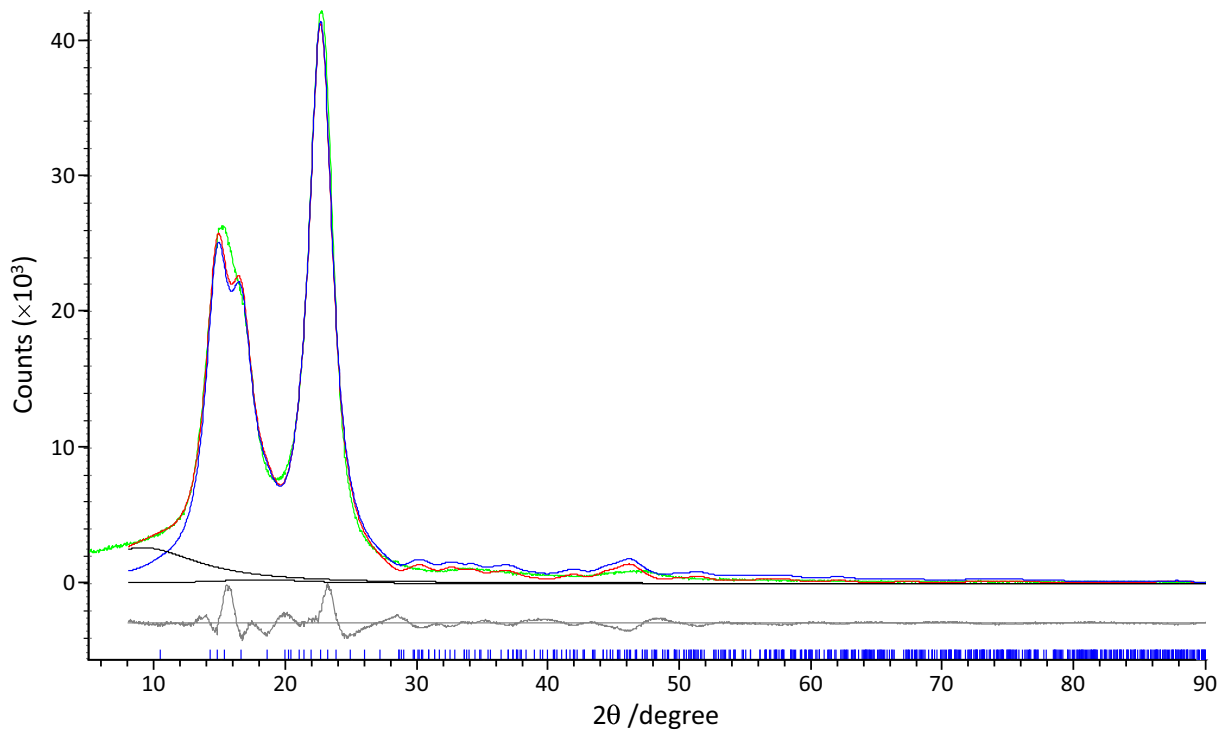


**Fig. 9** X-ray diffraction spectrum for a CNC thin film after background correction and deconvolution

in the sample or different sample preparation effects) contribute to the measurement uncertainty. Samples sonicated with varying total energies show similar size distributions for individual particles, although the number of clusters/image decreases with applied sonication energy based on DLS measurements. The similar size of individual particles, independent of sonication to disrupt agglomerates, suggests that the individual particles comprising the agglomerates have a similar size distribution to the individual suspended particles. The results indicate that the agglomerated particles observed by either AFM or TEM are a mixture of agglomerates present in the initial suspension and those formed by sample deposition on the mica slide or TEM grid.

It would be highly advantageous to implement automated image analysis procedures for CNCs. This would substantially decrease the time required to analyze large data sets; the manual analysis procedures used here take significantly (up to five times) longer than the data acquisition. In addition, automated procedures have the potential to eliminate the analyst bias in the analysis and may provide additional measurands that can be used to test for differences between distributions for different samples. Despite these advantages, automation is challenging for the irregular-shaped and agglomerated

CNCs for both AFM and TEM and, for TEM, the problem is exacerbated by the poor contrast, even for stained samples.

The TEM results clearly highlight the importance of a sufficiently large data set in order to adequately define the particle size distribution and suggest that differences in lab procedures may lead to variability in the results. A larger number of participating labs and a more detailed protocol would be needed to address this in more detail. The approximately twofold difference in cross section when comparing AFM height and TEM width may indicate significant lateral association of CNCs, particularly in the TEM samples. Similar observations of lateral association of CNCs in TEM images have also been reported in several recent studies using TEM and small-angle neutron scattering (Elazzouzi-Hafraoui et al. 2008; Kaushik et al. 2014; Cherhal et al. 2015; Uhlig et al. 2016). Particle size and surface charge and the presence of added salt influenced the degree of association, and in one case it was concluded that the uranyl acetate staining procedure promoted the formation of laterally associated CNCs (Kaushik et al. 2014). The crystallite size determined from X-ray diffraction (4.8 nm) is larger than the mean AFM height but significantly smaller than the TEM width, which

also provides some evidence for “counting” a larger number of laterally associated CNCs in the TEM images, since a rectangular cross section is not expected for wood pulp CNCs (Moon et al. 2011). Strictly speaking, crystallite size, as determined by XRD and if requirements for proper sample preparation are followed, provides a more accurate measurement of the size of individual crystallites than AFM or TEM. The CNCs extracted from wood pulp by acid hydrolysis may contain more than one individual crystallite, leading to a larger cross section, and the sample preparation for microscopy may also lead to agglomeration of individual CNCs. Further experiments aimed at analysis of CNCs fractionated by asymmetric flow field flow fractionation (Mukerjee and Hackley 2017) may provide some insight on the extent of agglomeration.

**Acknowledgements** Support for aspects of this work from NRCan’s Forest Innovation program is gratefully acknowledged. We thank Drs. Stephanie Beck and Jean Bouchard from FPInnovations, Montreal, for many useful discussions on CNC dispersion and characterization and CelluForce, Inc., Windsor, QC, for providing CNCs to produce the reference material. The content of this publication does not necessarily reflect the views or policies of the Department of Health and Human Services, nor does mention of trade names, commercial products, or organizations imply endorsement by the U.S. Government.

**Funding information** This study was partially funded by NRCan’s Forest Innovation Program (NRC contributors) and by National Institutes of Health (National Cancer Institute contributors, Contract No. HHSN261200800001E).

#### Compliance with ethical standards

**Conflict of interest** The authors declare that they have no conflict of interest.

#### References

- Babick F, Mielke J, Wohlleben W, Weigel S, Hodoroaba V-D (2016) How reliably can a material be classified as a nanomaterial? Available particle sizing techniques at work. *J Nanopart Res* 18:158
- Beck S, Bouchard J, Berry R (2011) Controlling the reflection wavelength of iridescent solid films of nanocrystalline cellulose. *Biomacromolecules* 12:167–172
- Beck S, Bouchard J, Berry R (2012) Dispersibility in water of dried nanocrystalline cellulose. *Biomacromolecules* 13: 1486–1494

- Bonevich JE, Haller WK (2010) Measuring the size of nanoparticles using transmission electron microscopy. NIST-NCL Joint Assay Protocol, PCC-7, Washington, DC
- Brinkmann A, Chen M, Couillard M, Jakubek ZJ, Leng T, Johnston LJ (2016) Correlating cellulose nanocrystal particle size and surface area. *Langmuir* 32:6105–6114
- Cherhal F, Cousin F, Capron I (2015) Influence of charge density and ionic strength on the aggregation process of cellulose nanocrystals in aqueous suspension, as revealed by small-angle neutron scattering. *Langmuir* 31:5596–5602
- Davis CS, Moon RJ, Ireland S, Foster EJ, Johnston LJ, Shatkin JA, Nelson K, Forster AM, Postek MT, Vladar AE, Gilman JW (2015) NIST-TAPPI workshop on measurement needs for cellulose nanomaterials. NIST Special Publication #1192. doi: <https://doi.org/10.6028/NIST.SP.1192>
- De Temmerman P-J, Lammertyn J, De Ketelare B, Kestens V, Roebben G, Verleysen E, Mast J (2014) Measurement uncertainties of size, shape, and surface measurements using transmission electron microscopy of near-monodisperse, near-spherical nanoparticles. *J Nanopart Res* 16:2177
- Delvallee A, Feltin N, Ducourtieux S, Trabelsi M, Hochepeid JF (2016) Toward an uncertainty budget for measuring nanoparticles by AFM. *Metrologia* 53:41–50
- Dufresne A (2013) Nanocellulose: a new ageless bionanomaterial. *Mater Today* 16:220–227
- Eichhorn S (2011) Cellulose nanowhiskers: promising materials for advanced applications. *Soft Matter* 7:303–315
- Elazzouzi-Hafraoui S, Nishiyama Y, Putaux J-L, Heux L, Dubreuil F, Rochas C (2008) The shape and size distribution of crystalline nanoparticles prepared by acid hydrolysis of native cellulose. *Biomacromolecules* 9:57–65
- Grulke EA, Yamamoto K, Kumagi K, Hausler I, Osterle W, Ortel E, Hodoroaba V-D, Brown SC, Chan C, Zheng J, Yamamoto K, Yashiki K, Song NW, Kim YH, Stefaniak AB, Schwegler-Berry D, Coleman VA, Jamting AK, Hermann J, Arakawa T, Burchett WW, Lambert JW, Stromberg AJ (2017) Size and shape distributions of primary crystallites in titania aggregates. *Adv Powder Technol* 28:1647–1659
- Guan X, Cueto R, Russo P, Qi Y, Wu Q (2012) Asymmetric flow field-flow fractionation with multiangle light scattering detection for characterization of cellulose nanocrystals. *Biomacromolecules* 13:2671–2679
- Hamad WY, Hu TQ (2010) Structure-property-yield interrelationships in nanocrystalline cellulose extraction. *Can J Chem Eng* 88:392–402
- Hoo CM, Doan T, Starostin N, West PE (2010) Optimal sample preparation for nanoparticle metrology (statistical size measurements) using atomic force microscopy. *J Nanopart Res* 12:939–949
- Hu Y, Abidi N (2016) Distinct nematic self-assembling behavior caused by different size-unified cellulose nanocrystals via a multistage separation. *Langmuir* 32:9863–9872
- ISO (19716:2016) Characterization of cellulose nanocrystals
- Jiang F, Esker AR, Roman M (2010) Acid-catalyzed and solvolytic desulfation of H<sub>2</sub>SO<sub>4</sub>-hydrolyzed cellulose nanocrystals. *Langmuir* 26:17919–17925
- Kaushik M, Chen WC, van de Ven TGM, Moore A (2014) An improved methodology for imaging cellulose nanocrystals by transmission electron microscopy. *Nord Pulp Pap Res J* 29:77–84

- Klemm D, Kramer F, Moritz S, Lindstrom T, Ankerfors M, Gray D, Dorris A (2011) Nanocelluloses: a new family of nature-based materials. *Angew Chem Int Ed Engl* 50:5438–5466
- Kovacs T, Naishi V, O'Connor B, Blaise C, Gagnez F, Hall L, Trudeau V, Martel P (2010) An ecotoxicological characterization of nanocrystalline cellulose (NCC). *Nanotoxicology* 4: 255–270
- Meli F, Klein T, Buhr E, Frase CG, Gleber G, Krumrey M, Duta A, Duta S, Korpelainen V, Bellotti R, Picotto GB, Boyd RD, Cuenat A (2012) Traceable size determination of nanoparticles, a comparison among European Metrology Institutes. *Meas Sci Technol* 23:125005
- Moon RJ, Martini A, Nairn J, Simonsen J, Youngblood J (2011) Cellulose nanomaterials review: structure, properties and nanocomposites. *Chem Soc Rev* 40:3941–3994
- Mukerjee A, Hackley VA (2017) Separation and characterization of cellulose nanocrystals by multi-detector asymmetric flow field-flow fractionation. *Analyst* 143:731–740
- Postek MT, Vladar A, Dagata J, Farkas N, Ming B, Wagner R, Raman A, Moon RJ, Sabo R, Wegner TH, Beecher J (2011) Development of the metrology and imaging of cellulose nanocrystals. *Meas Sci Technol* 22:024005
- Reid MS, Villalobos M, Cranston ED (2017) Benchmarking cellulose nanocrystals: from the laboratory to industrial production. *Langmuir* 33:1583–1598
- Rice SB, Chan C, Brown SC, Eschbach P, Han L, Esnor DS, Stefaniak AB, Bonevich J, Vladar AE, Hight Walker AR, Zheng J, Starnes C, Stromberg A, Ye J, Grulke EA (2013) Particle size distributions by transmission electron microscopy: an interlaboratory comparison case study. *Metrologia* 50: 663–678
- Shafiei-Sabet S, Hamad WY, Hatzikiriakos SG (2012) Rheology of nanocrystalline cellulose aqueous suspensions. *Langmuir* 28:17124–17133
- Shatkin JA, Kim B (2015) Cellulose nanomaterials: life cycle risk assessment and environmental health and safety roadmap. *Environ Sci Nano* 2:477–499
- Shatkin JA, Wegner TH, Bilek EM, Cowie J (2014) Market projections of cellulose nanomaterial-enabled products—part 1: applications. *TAPPI J* 13:9–16
- Taurozzi JS, Hackley VA, Wiesner MR (2011) Ultrasonic dispersion of nanoparticles for environmental, health and safety assessment—issues and recommendations. *Nanotoxicology* 5:711–729
- Trache D, Hussin MH, Haafiz MKM, Thakur VK (2017) Recent progress in cellulose nanocrystals: sources and production. *Nanoscale* 9:1763–1786
- Uhlig M, Fall A, Wellert S, Lehmann M, Prévost S, Wågberg L, von Klitzing R, Nyström G (2016) Two-dimensional aggregation and semidilute ordering in cellulose nanocrystals. *Langmuir* 32:442–450